WILEY | Hindawi

Research Article

Prediction of Fish Migration Caused by Ocean Warming Based on SARIMA Model

Feng Xu (iD),[1] **Yu-Ang Du** (iD),[1] **Hong Chen** (iD),[2] **and Jia-Ming Zhu** (iD)[1]

[1]*School of Statistics and Applied Mathematics, Anhui University of Finance & Economics, Bengbu 233030, China*
[2]*School of Languages and Media, Anhui University of Finance and Economics, Bengbu 233030, China*

Correspondence should be addressed to Jia-Ming Zhu; zhujm1973@163.com

Herring and mackerel are two of the most important pillars of Scottish fisheries. In recent years, global warming has caused a gradual rise in ocean temperatures. In order to survive and reproduce, herring and mackerel populations will migrate. This will have a huge impact on Scotland's fisheries. Therefore, we need to predict the relocation of fish stocks in advance, make timely adjustments to the fishing range, and minimize the loss of the fishing industry. In this article, we subdivide the research target sea area into 39 regions, establish the optimal SARIMA model for each region based on the collected seawater temperature time series data, and take region 13 and region 15 as examples to fit the ARIMA (3, 3, 1) (1, 2, 1) and ARIMA (2, 3, 1) (0, 2, 1) models with a period of 12. The results show that the SARIMA model fits well in all regions and predicts the temperature changes in the studied sea area from 2021 to 2050. Finally, according to the predicted sea temperature in different periods, the migration position of the fish school is predicted.

1. Introduction

Scotland is the largest marine fishery country in the United Kingdom. In 2020, the landing volume of Scottish caught fish products increased by 32.7% to 600 million pounds. As a specialty of Scotland, herring and mackerel have increased their output value by 42.8%, having extremely important economic significance. Many fishing companies in Scotland depend on them for a living. However, with the advancement of industrialization, the global greenhouse gas concentration has increased rapidly, and the ocean has absorbed a large amount of heat and atmospheric gases. Data from NOAA shows that the average temperature of the global ocean surface has increased by approximately 0.13°C every 10 years in the past 100 years. The change of global ocean average temperature is shown in Figure 1. Since 2015, the Northeast Atlantic Ocean in Scotland has risen by 0.048°C per year [1–7]. Marine organisms often live in relatively stable temperature environments and are very sensitive to temperature changes. Because this will directly affect its survival, metabolism, reproduction, development, and immune response, which will lead to the migration of habitats of marine life near Scotland, especially herring and mackerel

[8–12]. This is undoubtedly a crisis for a large number of small Scottish fishing companies. Due to the lack of advanced refrigeration technology and ships, coupled with the changes in the location of the fish stocks, it will greatly increase the difficulty of fishing and face the danger of insufficient fuel. It will cause great losses to the fishing industry in Scotland. Therefore, we urgently need a method that can accurately predict the migration location of herring and mackerel in order to minimize the losses of the fishery company and improve fishing efficiency.

2. Research Ideas

In order to accurately predict the migration location of herring and mackerel in the waters near Scotland, we first need to understand the marine environment suitable for herring and mackerel. The outline drawing of herring and mackerel is shown in Figure 2. By consulting related literature, we learned that herring and mackerel live in shallow waters. The temperature suitable for the growth of herring is about 8.8~9.8°C and for mackerel is about 8.86~9.6°C [11, 13–16]. According to the authoritative data of the Scottish Navy, the herring near Scotland in 2019 is mainly
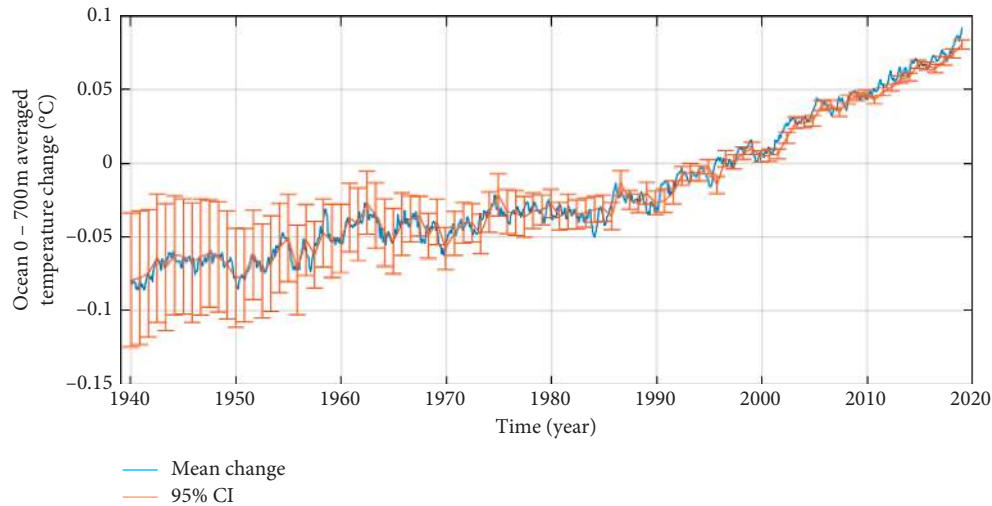
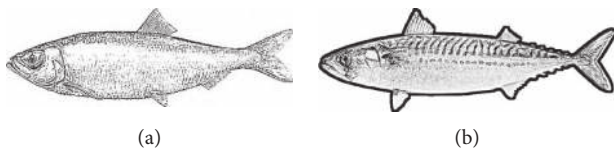FIGURE 1: The map of global ocean average temperature change.

FIGURE 2: Herring and mackerel.

distributed around (1.3°W, 60°N), and the mackerel is mainly distributed around (5°E, 58.5°N) and (0°E, 58.5°N). The main distribution areas of herring and sturgeon in England are shown in Figure 3.

Secondly, over time, the global ocean temperature is gradually changing. We need to predict the changes in sea temperature within the maximum distance that herring and mackerel fish can migrate [17–21]. Therefore, the scope of the sea area we studied is shown in Figure 4. At the same time, since the seawater temperature will change with the changes in latitude and longitude, in Figure 5, we subdivided the target research sea area into 39 regions, each of which is a rectangle with a width of 2.5 latitude and a length of 5 longitude. And we take the seawater temperature at the center of each region as the average seawater temperature in each region. Finally, the temperature change of the target sea area from 2021 to 2050 is predicted.

For the prediction of ocean temperature changes, we use the seasonal ARIMA time series model, which can effectively predict the overall seasonal temperature changes in the target sea area in the next 30 years [22–27], and then we can determine the future annual average temperature of the target sea area and compare it with the suitable ocean temperature for herring and mackerel; we can get the target migration position of the future fish school.

3. Problem Sources and Model Assumptions

The question studied in this article comes from the A question of the 2020 American College Students Mathematical Contest in Modeling. In order to ensure the rigor of the research, we
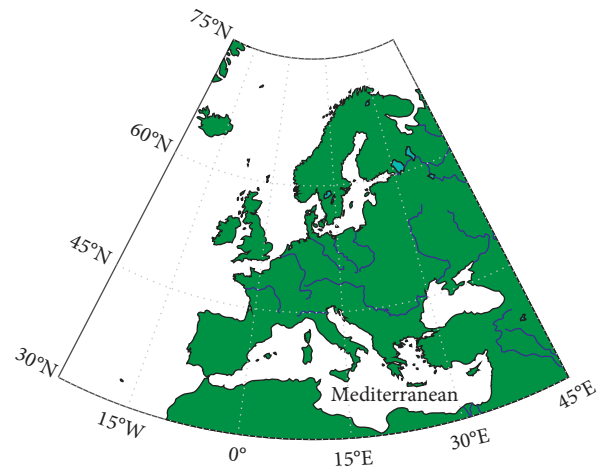

FIGURE 3: Main distribution areas of herring and sturgeon.

also need to make the following assumptions to eliminate the interference of other factors on the research results: (i) it is assumed that the seawater temperature changes are only affected by the seasonal changes of its own ocean currents and the greenhouse gas effect. (ii) It is assumed that the migration of fish schools is only affected by changes in sea temperature and not affected by other environmental factors, such as waste discharge, natural enemies, and other factors. (iii) It is assumed that the suitable living temperature of herring and mackerel schools is always constant, and there will be no mutations due to environmental changes. (iv) Suppose that, in the next 30 years, the global warming problem will not be significantly improved. The temperature change of the seawater will not be affected by policies such as limiting the emission of greenhouse gases [28–30].

4. SARIMA Model and Data Selection

4.1. SARIMA Model. The SARIMA model, the seasonal autoregressive integrated moving average model, is the introduction of seasonal terms in the ARIMA model, denoted
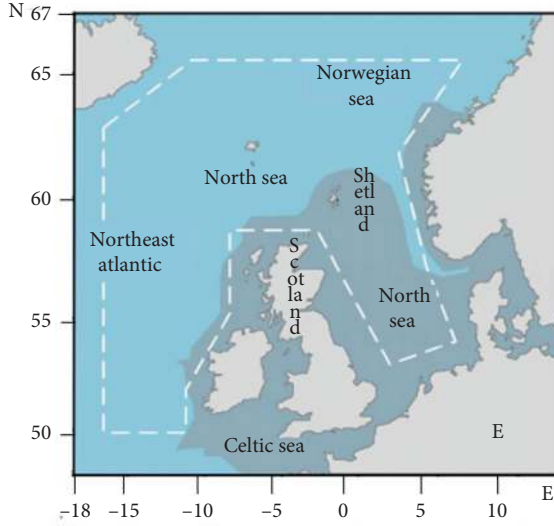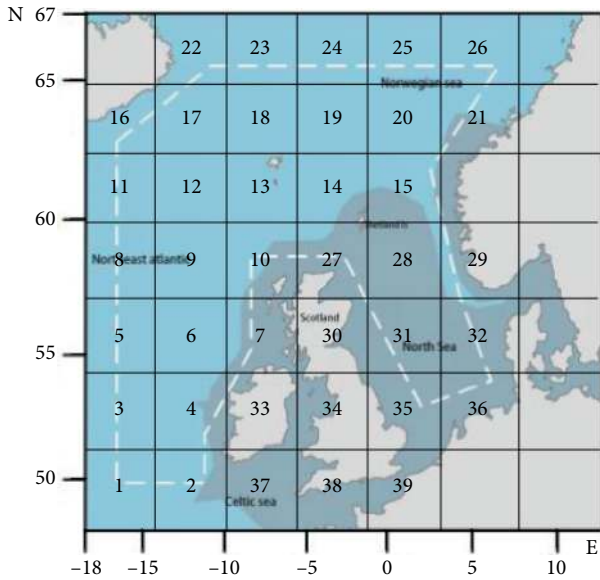
FIGURE 4: Target research area.

FIGURE 5: Target research sea area segmentation.

as ARIMA (p, d, q) (P, D, Q) s, where p, d, and q represent the parameters of the nonseasonal part of the model. P, D, and Q represent the parameters of the seasonal part of the model, and s is the seasonal period. Since the temperature of seawater is affected by not only long-term greenhouse gas emissions but also seasonal changes due to fluctuations in climate and ocean currents; we constructed a 12-month SARIMA model to study future temperature changes in the target sea area and predict the migration position of the fish school [31–40]. The model building process is as follows:

$$\begin{cases} \phi(B)\nabla^d X_t = \Theta(B)\varepsilon_t, \\ E(\varepsilon_t) = 0, \text{Var}(\varepsilon_t) = \sigma^2, E(\varepsilon_t \varepsilon_x) = 0, s = 12, \\ E(X, \varepsilon_t) = 0, \forall s < t, \end{cases} \quad (1)$$

in the above formula:

$$\nabla^d = (1 - B)^d, \quad (2)$$

where B is the delay operator and $\nabla^d X_t$ is the time series after finite-order difference. ε_t is the white noise sequence, $\Theta(B)$ is the stable and reversible ARMA (p, q) model's moving smoothing coefficient polynomial, and $\Phi(B)$ is the stationary and reversible ARMA (p, q) model's autoregressive coefficient polynomial.

Expressed as a linear function of preliminary observations,

$$X^t = \varepsilon_t + \psi_1 \varepsilon_{t-1} + \psi_2 \varepsilon_{t-2} + \cdots = \varphi(B)\varepsilon_t, \quad (3)$$

where the values of ψ_1 and ψ_2 are determined by the following equation:

$$\phi_B (1 - B)^d \psi(B) = \theta(B). \quad (4)$$

If $\Phi^*(B)$ is defined as a generalized autocorrelation function, we have

$$\phi^*(B) = \psi(B)(1 - b)^d = 1 - \phi_1 B - \phi_2 B^2 - \cdots. \quad (5)$$

It is easy to verify that the values of ψ_1, $\psi_2 \ldots$ satisfy the following recurrence formula:

$$\begin{cases} \psi_1 = \phi_1 - \theta_1, \\ \psi_2 = \phi_1 \psi_1 + \phi_2 - \theta_2, \\ \cdots, \\ \psi_j = \phi_1 \psi_{j-1} \cdots + \phi_{p+d} \psi_{j-p+d} - \theta_j. \end{cases} \quad (6)$$

In this formula,

$$\psi_j = \begin{cases} 0, & j < 1, \\ 1, & j = 0, \end{cases} \quad (7)$$

where j is the autoregressive coefficient and θ_j is the moving average coefficient. Then, the predicted temperature value of each area is expressed as follows:

$$X_{I+1} = (\varepsilon_{i+1} + \psi_i \varepsilon_{i+l-1} + \cdots + \psi_{l-1} \epsilon_{t+1}) + (\psi_i \varepsilon_t + \psi_{l+1} \varepsilon_{i-1} + \cdots). \quad (8)$$

Therefore, the SARIMA model is expressed as

$$\nabla^d \nabla_s^D x_t = \frac{\Theta(B)\Theta_s(B)}{\phi(B)\phi_s(B)} \varepsilon_t, \quad (9)$$

where $\phi_s(B) = 1 - \varphi_1 B^s - \cdots - \varphi_p B^{ps}$; $\Theta(B) = 1 - \theta_1 B - \cdots - \theta_q B^q$; and $\Theta_s(B) = 1 - \theta_1 B^s - \ldots - \theta_p B^{QS}$.

After the model is established, the model needs to be tested for adaptability, that is, whether the residual sequence of the model is a white noise sequence. If the residual sequence of the model is a white noise sequence, the model passes the white noise sequence to represent the model's information extraction of the time series. Sufficiently, the fitting effect to historical data is good, in line with the trend

of time series development; otherwise, the model needs to be optimized and the data refitted.

4.2. Data Analysis and Processing. This paper selects the monthly average water temperature data in shallow waters from 2004 to 2020 in the seas near Scotland and part of the North Atlantic Ocean (target research sea area) and converts them into fixed-base data. The data comes from the Scottish Marine Information Agency and the UK Met Office network.

We use the above data to establish the SARIMA model and use the reserved data to test the accuracy of the model. All data processing is completed by Ri386 4.0.2.

5. Empirical Analysis of Temperature Changes in the Research Sea Area

5.1. Model Identification and Establishment. We draw the autocorrelation and partial autocorrelation diagrams of the seawater temperature series (CST) at the center of each region. The 12-order delayed autocorrelation and partial autocorrelation coefficients are significantly larger than 2 times the standard deviation range and are significantly not 0. Therefore, the seawater temperature series in various regions are seasonal, with a 12-month cycle. In order to eliminate the seasonality of the sequence, we performed the first-order difference of the period length of $S = 12$ on the seawater temperature series at the center of each region, and the differenced sequence was recorded as SCST. Figures 6 and 7 are time series diagrams of the seawater temperature data of region 13 and area 15 after first-order difference. Figures 8–11 are the diagrams showing the relationship between autocorrelation and partial autocorrelation of SCST in region 13 and region 15. It can be seen from Figures 8–11 that after the first-order seasonal difference, the seasonality is greatly reduced, but not completely eliminated. Therefore, we carry out the second-order difference but still cannot eliminate it, so we still only carry out the first-order difference. It has been verified that all regions meet this characteristic.

Taking regions 13 and 15 as examples, it can be seen from Figures 8–11 that, in one cycle of the SCST of region 13, the number of partial autocorrelations that are significantly not 0 is 3 ($K = 1$, $K = 8$, $K = 9$), so consider choosing $p = 13$; the number of autocorrelations that are significantly not 0 is 3 ($K = 1$, $K = 2$, $K = 7$); consider choosing $q = 3$; and when $K = 12$, the partial autocorrelation coefficient is not significantly 0, so choose $P = 1$; when $K = 12$, $K = 24$, the autocorrelation coefficient is significantly not 0. So, choose $Q = 2$.

In one cycle of SCST in area 15, the number of partial autocorrelations that are significantly not 0 is 2 ($K = 1$, $K = 8$), so consider choosing $p = 2$; the number of autocorrelations that are significantly not 0 is 3 ($K = 1$, $K = 2$, $K = 7$); consider choosing $q = 3$; when $K = 12$, the partial autocorrelation coefficient is significantly close to 0, so choose $P = 0$; when $K = 12$, and $K = 24$ when the autocorrelation coefficient is significantly not 0. So, choose $Q = 2$.

Therefore, the primary model for region 13 is ARIMA (3, 3, 1) (1, 2, 1), ARIMA (2, 3, 1) (1, 2, 1), ARIMA (3, 4, 1) (1, 2, 1). The primary model for region 15 is ARIMA (2, 3, 1) (0, 2, 1), ARIMA (2, 4, 1) (0, 2, 1), and ARIMA (2, 5, 1) (0, 2, 1). After the model is initially selected, the parameter significance test of the model is carried out, and the optimal model is selected according to the minimum AIC index criterion. After comparative analysis, the optimal model for area 13 is ARIMA (3, 3, 1) (1, 2, 1); the optimal model for area 15 is ARIMA (2, 3, 1) (0, 2, 1). By analogy, we obtained the optimal seasonal model for all regions according to this method.

5.2. Model Test. In order to determine whether the seasonal model is effective, we need to test whether the residual sequence of the seasonal model in each region is a white noise sequence. If the residual sequence is a white noise sequence, it means that the model has fully extracted the information contained in the data, and the seasonal model has passed the adaptability test. We use the Q statistic to test the correlation of the model residual series. After testing, the autocorrelation and partial autocorrelation coefficients of each lag order of the optimal seasonal model in each region are close to 0. And the P values are all greater than 0.94, indicating that the residual sequence is a white noise sequence. Therefore, the optimal seasonal model in each region has passed the test, and the model is significantly established and can be used to predict the temperature change of seawater.

5.3. Model Prediction. Use the obtained optimal seasonal model for each region to fit and predict the monthly average shallow sea temperature in each region from January 2021 to December 2050. Take area 13 and area 15 as examples and use R software to fit seasonal models ARIMA (3, 3, 1) (1, 2, 1) and ARIMA (2, 3, 1) (0, 2, 1), sequence diagram as shown in Figures 12 and 13.

5.4. The Location of Fish Migration. Because herring and mackerel live in seas with relatively stable temperatures, they will not migrate with seasonal temperature changes but will only migrate due to changes in the overall temperature of the sea. Therefore, we need to calculate the annual average sea temperature of each region in the next 30 years. The formula is

$$T_{jk} = \frac{1}{s} \sum_{i=1}^{n=12} T'_{jk}, \quad j = 1, 2, \ldots, 39, k = 1, 2, \ldots, 30. \quad (10)$$

Among them, $s = 12$, T_{jk} is the annual average sea temperature of the jth area in the kth year and T'_{jki} is the predicted average sea temperature of the "j"$^{\text{th}}$ area in the "i"$^{\text{th}}$ month of the "k"$^{\text{th}}$ year. After calculation, the annual average sea temperature of each area of the study sea area in 2030, 2040, and 2050 is shown in Figures 14–16.

It can be seen from Figures 14–16 that the temperature of the sea near Scotland gradually rises and increases with time.
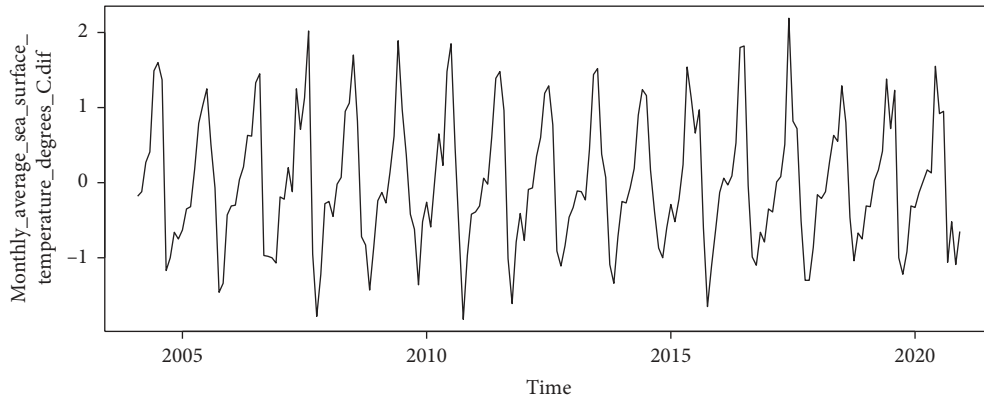
Figure 6: The time series diagram of the seawater temperature data of region 13 after first-order difference.
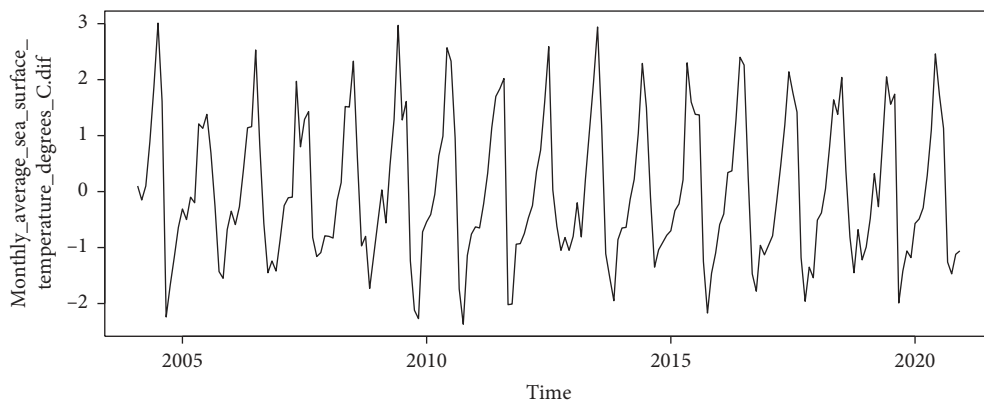

Figure 7: The time series diagram of the seawater temperature data of region 15 after first-order difference.
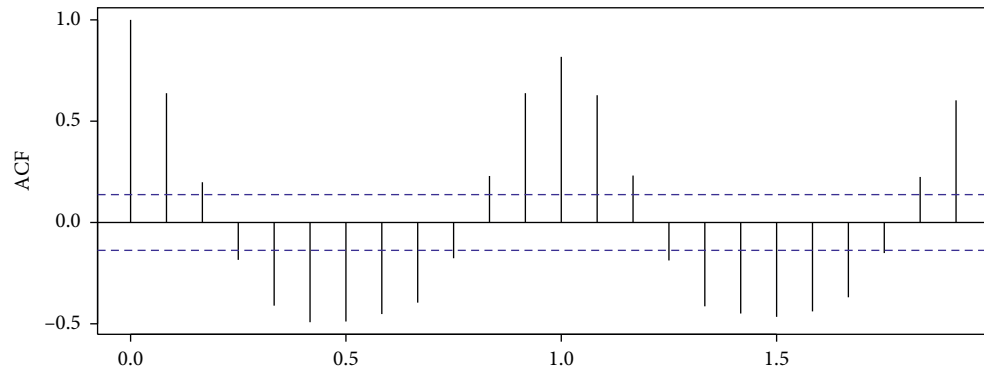

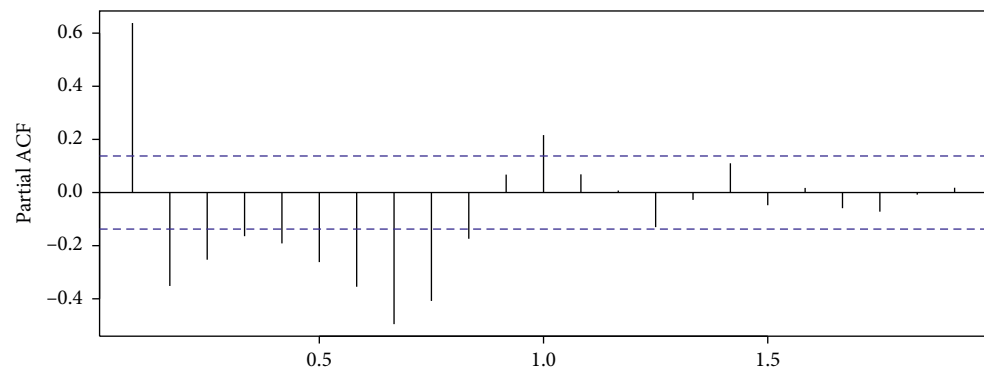Figure 8: The autocorrelation diagram of SCST in region 13 (ACF).

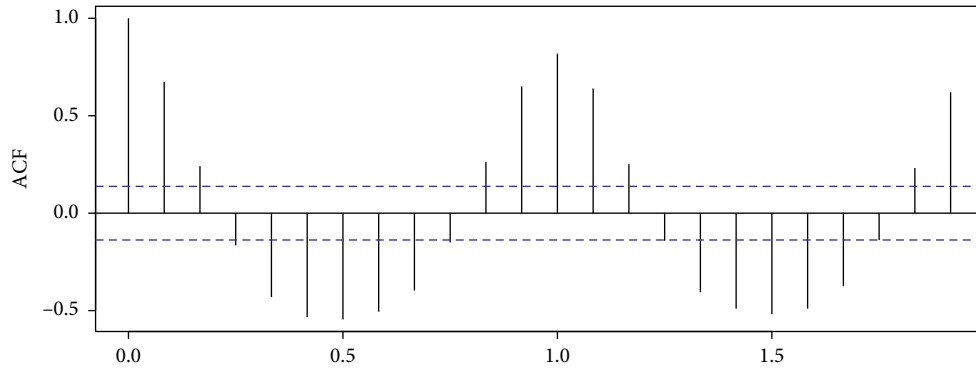Figure 9: The partial autocorrelation diagram of SCST in region 13 (PACF).

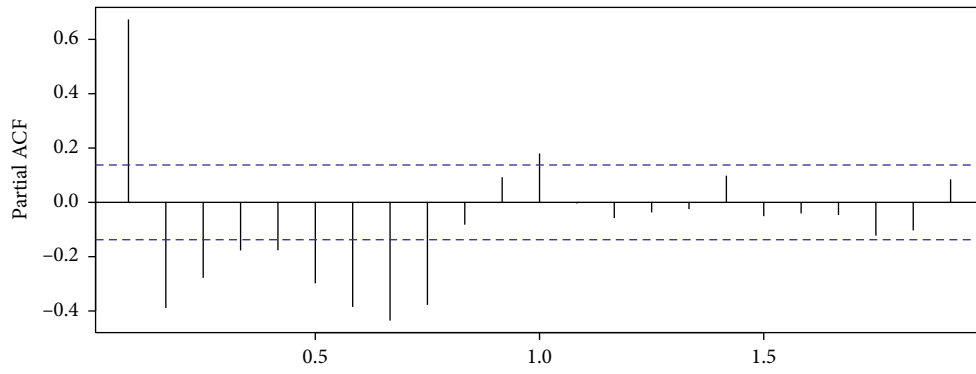Figure 10: The autocorrelation diagram of SCST in region 15 (ACF).

Figure 11: The partial autocorrelation diagram of SCST in region 15 (PACF).
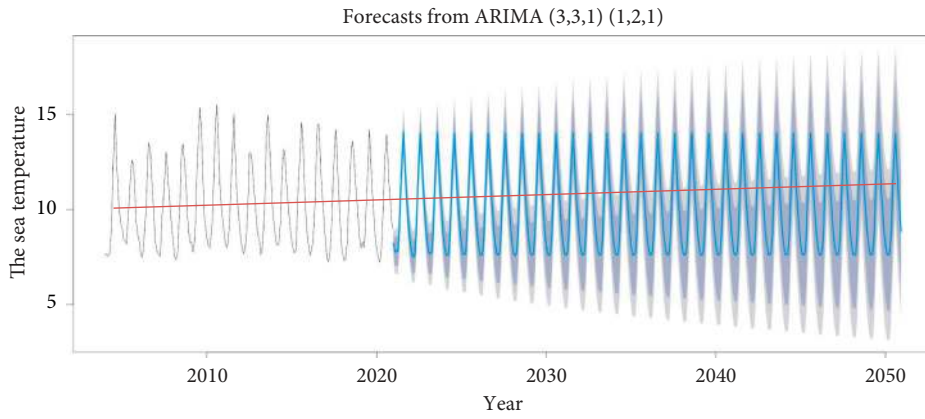

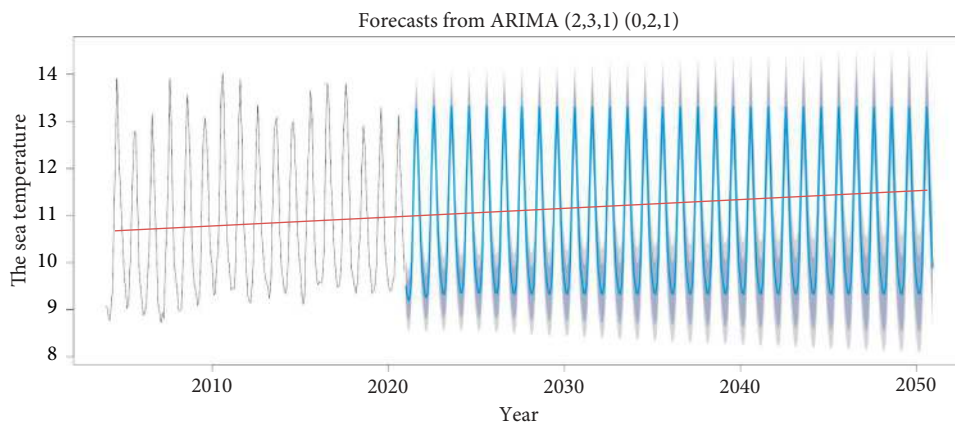Figure 12: Time series forecast of monthly average sea temperature in region 13.

Figure 13: Time series forecast of monthly average sea temperature in region 15.
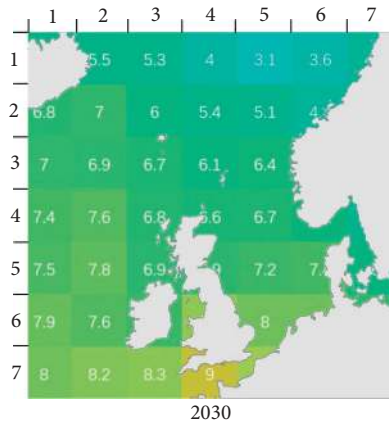
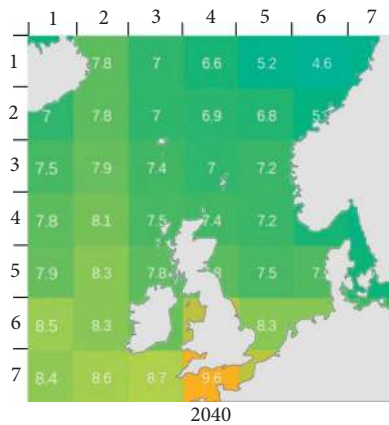Figure 14: The predicted annual average sea.

Figure 15: The predicted annual average sea temperature of the study area in 2030 temperature of the study area in 2040.
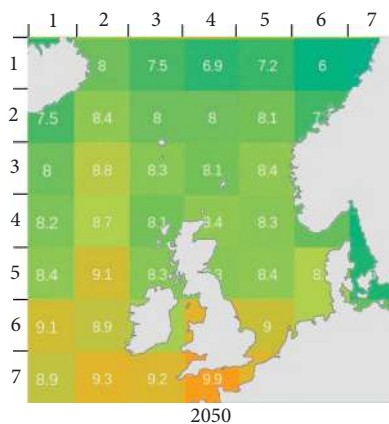

Figure 16: The predicted annual average sea temperature of the study area in 2050.

By 2030, the shallow water temperature in the northeastern Atlantic Ocean and the Norwegian Sea will reach 6.5 degrees and 4 degrees. By 2050, the temperature in these two regions will reach 7 degrees and 5 degrees, respectively. At the same

Table 1: Predicted migration positions of herring and mackerel.

Time	Herring		Mackerel	
2030	(2°W, 61°N)	(5°W, 58°N)	(9°E, 55°N)	(1°W, 54°N)
2040	(8°E, 64°N)	(2°W, 57°N)	(3°W, 62°N)	(9°E, 58°N)
2050	(2°E, 60°N)	(24°W, 58°N)	(9°E, 67°N)	(4°W, 62°N)
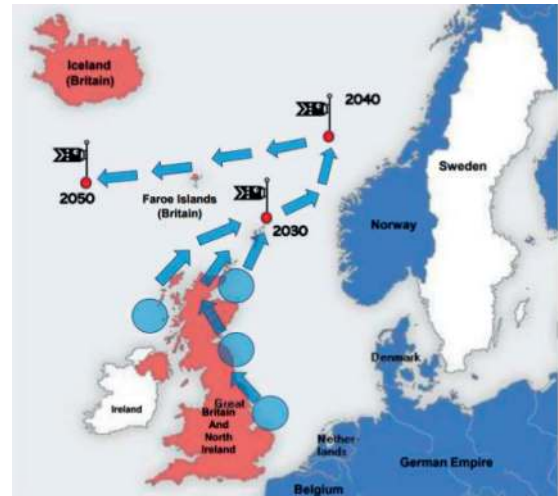
(a)
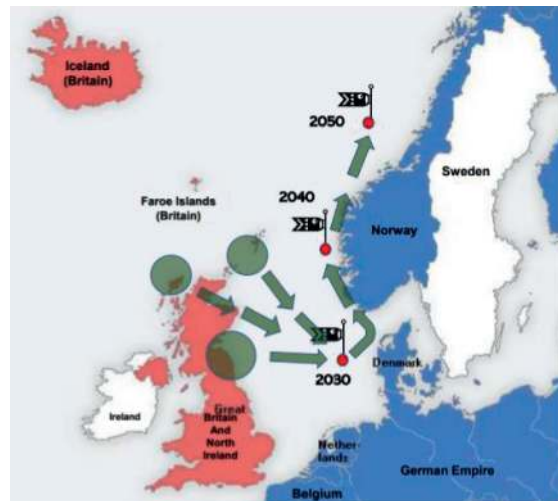
(b)

Figure 17: Predicted migration positions of herring and mackerel: (a) herring migration illustration and (b) mackerel migration illustration.

time, the temperature near the Celtic Sea and the English Channel will rise to 9 degrees.

From this, we can see that the temperature of the sea area where the herring and mackerel fish originally lived has changed, and with the increase of time, the range of changes will become greater and greater, it is no longer suitable for the survival of the fish, and the fish will migrate to a temperature suitable for the sea. Since the migration process of fish schools is very long, we consider that the

fish schools will have a complete migration activity once every ten years at an interval of 10 years and predict their migration locations. The results are shown in Table 1 and Figure 17.

6. Conclusion

Based on the characteristics of seawater temperature changes with latitude and longitude, the study area is subdivided into 39 regions, and the time series data of seawater temperature from January 2004 to December 2020 are used for modeling. By using the mature time series modeling technique, a hybrid seasonal model with high prediction accuracy is established for each region, such as ARIMA (3, 3, 1) (1, 2, 1) and ARIMA (2, 3, 1) (0, 2, 1) models for region 13 and region 15 and pass the white noise test. Based on the forecast results, we can see that the average annual sea temperature in the study area will rise continuously in the next 30 years, which will lead to the migration of herring and mackerel populations. According to the living environment of herring and mackerel, the future migration location of Shad was predicted accurately, and the migration route was planned. This would significantly improve the efficiency of Scottish small-scale fisheries with respect to herring and mackerel, reduce fishing costs, and minimize the heavy losses to the fishing industry caused by the migration of fish stocks, to further the development of Scotland's fishing industry.

Data Availability

The research question was taken from Question A of the 2020 Mathematical Contest in Modeling and Interdisciplinary Contest in Modeling (MCM/ICM), and the data were obtained from the Scottish Marine Information Agency and the UK Met Office Website.

Conflicts of Interest

The authors declare that there are no conflicts of interest regarding the publication of this paper.

Acknowledgments

References

[1] R. Barman, A. K. Jain, and M. Liang, "Climate-driven uncertainties in modeling terrestrial energy and water fluxes: a site-level to global-scale analysis," *Global Change Biology*, vol. 20, no. 6, pp. 1885–1900, 2014.

[2] R. S. Johnson, "Application of the ideas and techniques of classical fluid mechanics to some problems in physical oceanography," *Philosophical Transactions of the Royal Society A Mathematical Physical & Engineering Sciences*, vol. 376, no. 2111, pp. 1–19, 2018.

[3] P. Goertler, B. Mahardja, and T. Sommer, "Striped bass (*Morone saxatilis*) migration timing driven by estuary outflow and sea surface temperature in the San Francisco Bay-Delta, California," *Scientific Reports*, vol. 11, no. 1, pp. 1510.1–1510.11, 2021.

[4] V. A. Luchin and N. I. Grigoryeva, "The effects of water temperature on the timing of spawning and spat settlement of the yesso scallop (mizuhopecten yessoensis jay, 1857) in minonosok cove (posyet bay, peter the great bay, sea of Japan)," *Russian Journal of Marine Biology*, vol. 46, no. 7, pp. 580–589, 2021.

[5] K. Myrberg, S. Korpinen, and L. Uusitalo, "Physical oceanography sets the scene for the marine strategy framework directive implementation in the Baltic sea," *Marine Policy*, vol. 107, pp. 103591.1–103591.7, 2019.

[6] W. Yu, Y. Liu, X.-Q. Yang et al., "Impact of North Atlantic SST and Tibetan plateau forcing on seasonal transition of springtime south asian monsoon circulation," *Climate Dynamics*, vol. 56, no. 1-2, pp. 559–579, 2020.

[7] L. F. Borchert, A. Düsterhus, S. Brune, W. A. Müller, and J. Baehr, "Forecast-oriented assessment of decadal hindcast skill for North Atlantic SST," *Geophysical Research Letters*, vol. 46, no. 20, pp. 11444–11454, 2019.

[8] E. Serviere-Zaragoza, S. E. Lluch-Cota, A. Mazariegos-Villarreal, E. F. Balart, H. Valencia-Valdez, and L. C. Méndez-Rodríguez, "Cadmium, lead, copper, zinc, and iron concentration patterns in three marine fish species from two different mining sites inside the gulf of California, Mexico," *International Journal of Environmental Research and Public Health*, vol. 18, no. 2, pp. 844.1–844.18, 2021.

[9] Y. Wang, J. Gagnon, and S. Nair, "Herring milt protein hydrolysate improves insulin resistance in high-fat-diet-induced obese male C57BL/6J mice," *Marine Drugs*, vol. 17, no. 8, pp. 456.1–456.14, 2019.

[10] X. Pan, Z. Ye, B. Xu et al., "Combining otolith elemental signatures with multivariate analytical models to verify the migratory pattern of Japanese Spanish mackerel (*Scomberomorus niphonius*) in the southern yellow sea," *Acta Oceanologica Sinica*, vol. 39, no. 12, pp. 54–64, 2021.

[11] A. O. Zolotov, O. G. Zolotov, and Y. K. Kurbanov, "The status of the stock and the current fishery for the atka mackerel, pleurogrammus monopterygius (Pallas, 1810), in the Olyutorsky-Navarin area, Bering sea," *Russian Journal of Marine Biology*, vol. 46, no. 7, pp. 535–549, 2021.

[12] M. Tonezzer, "Detection of mackerel fish spoilage with a gas sensor based on one single SnO_2 nanowire," *Chemosensors*, vol. 9, no. 1, pp. 2.1–2.10, 2021.

[13] D. M. Campos, A. C. M. Rodrigues, R. J. M. Rocha et al., "Are microplastics impairing marine fish larviculture?-Preliminary results with argyrosomus regius," *Water*, vol. 13, no. 1, pp. 104.1–104.13, 2021.

[14] T. B. Zheltonozhskaya, N. M. Permyakova, O. O. Kravchenko et al., "Polymer/inorganic hybrids containing silver nanoparticles and their activity in the disinfection of fish aquariums/ponds," *Polymer-Plastics Technology and Materials*, vol. 60, no. 2, pp. 1–23, 2020.

[15] K. Lockhart, C. Irvine, J. MacLaurin et al., "Peregrine falcon scavenges adult herring gull at nest site on lake superior,

Ontario, Canada," *Journal of Raptor Research*, vol. 54, no. 4, pp. 470–472, 2020.

[16] S. M. Yusop, M. A. Mustapha, and T. Lihan, "Determination of spatio-temporal distribution of Rastrelliger kanagurta using modelling techniques for optimal fishing," *Journal of Coastal Conservation*, vol. 25, no. 1, pp. 1–17, 2021.

[17] R. Noori, M. R. Abbasi, J. F. Adamowski, and M. Dehghani, "A simple mathematical model to predict sea surface temperature over the northwest Indian Ocean," *Estuarine, Coastal and Shelf Science*, vol. 197, pp. 236–243, 2017.

[18] D. Pratiwi, S. M. U. Agustini, and W. Windasari, "Forecasting farmer exchange rate in bali Province using seasonal autoregressive integrated moving average (SARIMA) method," *Journal of Physics*, vol. 1503, no. 1, pp. 012002.1–012002.6, 2020.

[19] M. Sivaguru, L. G. Todorov, and C. E. Fouke, "Corals regulate the distribution and abundance of Symbiodiniaceae and biomolecules in response to changing water depth and sea surface temperature," *Scientific Reports*, vol. 11, no. 1, pp. 2230.1–2230.19, 2021.

[20] G. Bayable, G. Amare, and G. Alemu, "Spatiotemporal variability and trends of rainfall and its association with pacific ocean sea surface temperature in west harerge zone, eastern Ethiopia," *Environmental Systems Research*, vol. 10, no. 1, pp. 1–16, 2021.

[21] D. A. Iarovaya, V. V. Efimov, V. S. Barabanov, and A. A. Mizyuk, "Response of the black sea upper layer to the cyclone passage on September 25–29, 2005," *Russian Meteorology and Hydrology*, vol. 45, no. 10, pp. 701–711, 2021.

[22] R. W. Divisekara, G. J. M. S. R. Jayasinghe, and K. W. S. N. Kumari, "Forecasting the red lentils commodity market price using SARIMA models," *SN Business & Economics*, vol. 1, no. 1, pp. 1–13, 2021.

[23] M. Farsi, D. Hosahalli, B. R. Manjunatha et al., "Parallel genetic algorithms for optimizing the SARIMA model for better forecasting of the NCDC weather data," *Alexandria Engineering Journal*, vol. 60, no. 1, pp. 1299–1316, 2021.

[24] D. Kreuzer, M. Munz, and S. Schlüter, "Short-term temperature forecasts using convolutional neural network—an application to different weather stations in Germany," *Machine Learning with Applications*, vol. 2, no. 12, pp. 100007.1–10007.11, 2020.

[25] S. W. Lin, Y. S. Hung, W. C. Lee, and C. H. Liu, "Optimal collecting policy for apheresis platelets in a regional blood center," *Vox Sanguinis*, vol. 115, no. 2, pp. 148–158, 2020.

[26] K. Ruchir and R. Milind, "Pattern recognition—using sarima models for product sales analysis in time series forecasting," *Journal of Research in Science and Engineering*, vol. 2, no. 10, pp. 96–98, 2020.

[27] J. Gao, J. Li, and M. Wang, "Time series analysis of cumulative incidences of typhoid and paratyphoid fevers in China using both Grey and SARIMA models," *PLoS One*, vol. 15, no. 10, pp. e0241217.1–e0241217.14, 2020.

[28] R. Torres, J. Shutler, Y. Artioli et al., "Sensitivity of modeled CO_2 air–sea flux in a coastal environment to surface temperature gradients, surfactants, and satellite data assimilation," *Remote Sensing*, vol. 12, no. 12, pp. 2038.1–2038.29, 2020.

[29] V. Costas, M. Yuri, and E. Maria, "Paleoecological and recent data show a steady temporal evolution of carbon dioxide and temperature," *Atmospheric Pollution Research*, vol. 11, no. 4, pp. 714–722, 2020.

[30] J. Spackeen, R. Sipler, E. Bertrand et al., "Impact of temperature, CO_2, and iron on nutrient uptake by a late-season microbial community from the Ross Sea, Antarctica," *Aquatic Microbial Ecology*, vol. 82, no. 2, pp. 145–159, 2018.

[31] A. S. Olorunfemi and B. M. Ardo, "Modelling and forecasting seasonal behavior of rainfall in Abuja, Nigeria; A SARIMA approach," *American Journal of Mathematics and Statistics*, vol. 10, no. 1, pp. 10–19, 2020.

[32] K. Paisit and S. Krung, "Automatic SARIMA order identification convolutional neural network," *International Journal of Machine Learning and Computing*, vol. 10, no. 5, pp. 662–668, 2020.

[33] Z.-B. Zuo, M.-C. Wang, H.-Z. Cui et al., "Spatiotemporal characteristics and the epidemiology of tuberculosis in China from 2004 to 2017 by the nationwide surveillance system," *BMC Public Health*, vol. 20, no. 1, pp. 1284.1–1284.14, 2020.

[34] O. A. Samuel, M. Bello, and I. A. Auta, "Seasonal autoregressive integrated moving average (SARIMA) model for the analysis of frequency of monthly rainfall in Osun state, Nigeria," *Physical Science International Journal*, vol. 22, no. 4, pp. 1–9, 2019.

[35] S. Siswanto, R. Risva, and N. Marliana, "Epidemiology forecasting analysis of dengue haemorraghic fever with seasonal autoregressive integrated moving average in tropical area," *Public Health of Indonesia*, vol. 5, no. 2, pp. 38–47, 2019.

[36] J.-M. Zhu, A.-N. Li, N. Sun et al., "The cultivation of innovation ability of new economic and management talents in discipline competitions under the background of big data," *Frontiers in Educational Research*, vol. 3, no. 11, pp. 100–106, 2020.

[37] K. V. N. Murthy, R. Saravana, and K. Vijaya Kumar, "Stochastic modelling of the monthly average maximum and minimum temperature patterns in India 1981–2015," *Meteorology and Atmospheric Physics*, vol. 131, no. 4, pp. 775–787, 2019.

[38] T. H. Abebe, "Teshome hailemeskel abebe. Time series analysis of monthly average temperature and rainfall using seasonal ARIMA model (in case of ambo area, Ethiopia)," *International Journal of Theoretical and Applied Mathematics*, vol. 6, no. 5, pp. 76–87, 2020.

[39] S. Tamie and O. Yasushi, "Comparison of models for excess mortality of influenza applied to Japan," *Journal of Biosciences and Medicines*, vol. 7, no. 6, pp. 13–23, 2020.

[40] L. Martínez-Acosta, J. P. Medrano-Barboza, L. López-Ramos et al., "SARIMA approach to generating synthetic monthly rainfall in the Sinú river watershed in Colombia," *Atmosphere*, vol. 11, no. 6, pp. 602.1–602.16, 2020.